International Journal of Engineering, Mathematical and Physical Sciences
ISSN: 2517-9934
Vol:14, No:1, 2020

ROSA/LSTF Separate Effect Test on Natural Circulation under High Core Power Condition of Pressurized Water Reactor

Takeshi Takeda

***Abstract*—**A separate effect test (SET) simulated natural circulation (NC) under high core power condition of a pressurized water reactor (PWR) utilizing the ROSA/LSTF (rig of safety assessment/large-scale test facility). The LSTF test results clarified the relationship between the primary loop mass inventory and the primary loop mass flow rate being dependent on the NC mode at a constant core power of 8% of the volumetric-scaled PWR nominal power. When the core power was 9% or more during reflux condensation, large-amplitude level oscillation in a form of slow fill and dump occurred in steam generator (SG) U-tubes. At 11% core power during reflux condensation, intermittent rise took place in the cladding surface temperature of simulated fuel rods. The RELAP5/MOD3.3 code indicated the insufficient prediction of the SG U-tube liquid level behavior during reflux condensation.

***Keywords*—**LSTF, natural circulation, core power, RELAP5.

I. Introduction

HIGH reliability of control rods leads to relatively low risk for anticipated transient without scram of a light water reactor. The new regulatory requirements for the Japanese light-water nuclear power reactors [1] include the evaluation of the effectiveness of measures that should be taken to reduce the core power in the anticipated transient without scram. If no proper measures are taken despite failure of scram, relatively high core power will continue for a long time. This may result in counter-current flow limiting (CCFL) [2]-[4] at the inlet of SG U-tubes due to high steam velocity in a PWR. Safety concerns with the PWR involve a further drop in the core liquid level because of the difference in water head between the upflow and downflow sides of the SG U-tubes owing to the CCFL, as illustrated in Fig. 1.

By utilizing the ROSA/LSTF [5] of Japan Atomic Energy Agency, two integral effect tests (IETs) were conducted to make clear thermal-hydraulic phenomena specific to NC under high core power condition due to failure of scram. The LSTF is a full-height and 1/48 volumetrically-scaled two-loop system simulator of a Westinghouse (WH)-type four-loop 3,423 MW (thermal) PWR. The two IETs simulated a small-break loss-of-coolant accident without scram in 2006 [6], [7] or a loss-of-feedwater transient without scram with delayed actuation of auxiliary feedwater in 2007 [8]. The core power curves for the two IETs were determined on the basis of some calculations of the PWR with the RELAP5 code. Results of the two IETs have revealed the liquid accumulation in the SG U-tubes during reflux condensation due to the CCFL for high steam velocity.

Takeshi Takeda is with Nuclear Regulation Authority, Roppongi, Minato-ku, Tokyo 106-8450, Japan (phone: 81-3-5114-2100; fax: 81-3-5114-2179; e-mail: takeda.takeshi4695@gmail.com).

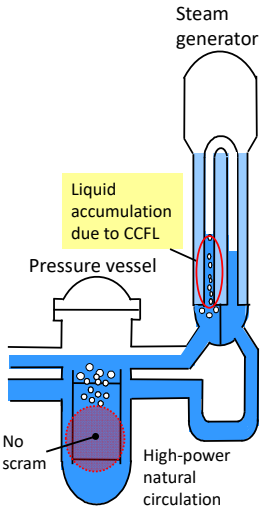

Fig. 1 Coolant distribution in reflux condensation mode during transient without scram of PWR

In order to evaluate the NC performance in the PWR systems, many experimental databases have been created from SETs utilizing integral test facilities with smaller volume compared to the LSTF. The integral test facilities used for the SETs included Semiscale [9], LOBI (loop off-normal behavior investigations) [10], BETHSY (boucle d'etudes thermohydraulique systeme) [11], IIST (institute of nuclear energy research integral system test) [12], SPES (simulatore PWR per esperienze di sicurezza) [13], PSB–VVER (polnomasshtabnyi stend besopasnosti – vodo-vodianoi energeticheskii reaktor) [14], PKL (primärkreisläufe versuchsanlage) [15], PACTEL (parallel channel test loop) [16], and ATLAS (advanced thermal-hydraulic test loop for accident simulation) [17]. Meanwhile, two SETs with the LSTF denoted as ST-NC-02 [18] and ST-NC-01 [19] were performed in 1985 simulating NC at fixed core power levels that correspond to 2% and 5% of the volumetric-scaled PWR nominal powers (1/48 × 3,423 MW), respectively. The 2% core power is representative of the NC during a PWR small-break loss-of-coolant accident [18]. However, there have been scarcely any experimental data with regard to the NC at over 5% of the volumetric-scaled PWR nominal power [20].

This study focused on an LSTF SET designated as ST-NC-27, which simulated PWR high-power NC in 2004. The author assessed the ST-NC-27 test while referring to the CSNI (committee on the safety of nuclear installation) matrix of the SETs as a guide for validating the thermal-hydraulic system codes [21], [22]. In the ST-NC-27 test, the primary loop mass inventory and the core power were selected as parameters. The SG secondary-side collapsed liquid level was kept at a certain liquid level above the SG U-tube height to simulate adequate injection of feedwater into the SG secondary-side. In order to examine the NC flow behavior at the reduced primary loop mass inventories under high core power condition, the primary loop mass inventory was decreased stepwise from the 100% initial value at a constant core power of 8%. The conditions for the SG secondary-side collapsed liquid level and the primary loop mass inventory change were defined based on those used for the ST-NC-02 and ST-NC-01 tests [18], [19]. Subsequently, the core power was raised in a stepwise manner from 8% during both two-phase NC and reflux condensation to investigate the influences of the core power on the SG U-tube liquid level behavior. The author was just trying to carry out further the posttest analysis of the ST-NC-27 test by employing the RELAP5/MOD3.3 code [23] paying attention to the SG U-tube liquid level behavior during reflux condensation (to be mentioned in Section III *C*). In the posttest analysis, the SG U-tubes were modeled by fine-mesh multiple parallel flow channels to evaluate the code predictive capability. This paper describes major observations in the ST-NC-27 test and the posttest calculation of the RELAP5 code.

II. Assessment of SET with LSTF

A. Outline of LSTF System

The LSTF composing of a pressure vessel, pressurizer, and primary loops is shown schematically in Fig. 2. Each loop has an active SG, primary coolant pump, and hot and cold legs. Loops with and without pressurizer are denoted as loop-A and loop-B, respectively. Each SG is furnished with 141 full-size U-tubes (inner-diameter of 19.6 mm, nine different lengths as mentioned in Table I), inlet and outlet plena, boiler section, steam separator, steam dome, steam dryer, main steam line, four downcomer pipes, and other internals. Six instrumented tubes for each SG consist of two short tubes (Type 1 in Table I) designated as Tubes 1 and 6, two medium tubes (Type 5) as Tubes 2 and 5, and two long tubes (Type 9) as Tubes 3 and 4. The LSTF core power is limited to 10 MW that is 14% of the volumetrically scaled PWR normal core power because of a limitation in the capacity of power supply. The axial profile of the core power is structured in a nine-step chopped cosine in which a peaking factor is 1.495.

B. Description of LSTF Test against Major Criteria to Select Appropriate SET

The major criteria to choose a suitable SET were defined in reference to the CSNI validation matrix of the SETs for the thermal-hydraulic system codes [21], [22]. While available documentation is one of criteria for the test selection mentioned in the CSNI validation matrix, no documents of the ST-NC-27 test have been reported. The foremost criteria involved geometry, scale, instrumentation, available measurements, range of main parameters, validation of complete system, and covered phenomena and models. Table II shows the description of the ST-NC-27 test against the major criteria.

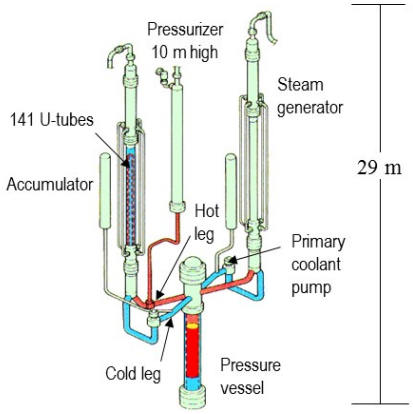

Fig. 2 Schematic view of ROSA/LSTF

TABLE I
Details of LSTF U-Tubes in each SG

Type	Straight Length (m)	Total Length (m)	Number of Tubes	Instrumented Tubes
1	9.44	19.04	21	Two short tubes
2	9.59	19.44	19	
3	9.74	19.84	19	
4	9.89	20.25	19	
5	10.04	20.65	17	Two medium tubes
6	10.19	21.06	15	
7	10.34	21.46	13	
8	10.49	21.86	11	
9	10.64	22.26	7	Two long tubes

As for the geometry, four primary loops of WH-type PWR are represented by two equal-volume loops to simulate two-phase flows. The dimensions of the full assembly are almost the same as those of the WH-type PWR 17 × 17 fuel assembly to preserve the heat transfer characteristics of the core. The core (active height of 3.66 m) is composed of 1,008 electrically heated rods in 24 rod bundles to simulate the fuel rod assembly in the WH-type PWR.

Regarding the scale [24], the design of the LSTF models the full-height primary system of the WH-type PWR. The volumetric scaling ratio of the primary loops is 1/48 of the WH-type PWR, which is the largest among the integral test facilities. Flow area in the horizontal legs is selected to conserve the ratio of the length to the square root of the pipe diameter of the WH-type PWR (Froude number basis) [25]. This approach is adopted to better simulate the flow regime transitions in the primary loops. The time scale of simulated phenomena is one to one to those in the WH-type PWR.

The LSTF has a large number of instruments, such as pressure transducer, differential pressure transducer, thermocouple, flow meter, level meter, gamma-ray

densitometer, and electric power meter. There are the available measurements, including pressure, differential pressure, fluid temperature, wall temperature, flow rate, liquid level, fluid density, and electric power. Table III shows the uncertainty of the LSTF test result for each of the major parameters (to be submitted in Figs. 3-18), which is estimated on the basis of the accuracy of the related instrument [5]. The measurement precision of the individual parameters is high enough to ensure the measured data consistency.

TABLE II
DESCRIPTION OF LSTF TEST AGAINST MAJOR CRITERIA TO SELECT APPROPRIATE SET

Criterion	LSTF Test (ST-NC-27)
Type	SET
Target scenario	NC under high core power condition
Working fluid	Steam/water
Material properties	Electrically heated rod cladding of Inconel 600 (density, specific heat, thermal conductivity), etc.
Component and/or reactor	Overall system of PWR
Geometry	1) Four primary loops of WH-type PWR are represented by two equal-volume loops. 2) Full assembly has mostly the same dimensions as those of WH-type four-loop PWR 17 × 17 fuel assembly. 3) Core (active height of 3.66 m) consists of 1,008 electrically heated rods in 24 rod bundles.
Scale	1) Full-height primary system of WH-type four-loop PWR is modeled. 2) Volumetric scaling ratio of primary loops is 1/48 of WH-type four-loop PWR. 3) Flow area in horizontal leg is scaled to conserve ratio of length to square-root of pipe diameter of WH-type four-loop PWR (Froude number basis). 4) Time scale of simulated phenomena is one to one to those in WH-type four-loop PWR.
Instrumentation	Pressure transducer, differential pressure, thermocouple, flow meter, level meter, gamma-ray densitometer, electric power meter, etc.
Available measurements	Pressure, differential pressure, fluid temperature, wall temperature, flow rate, liquid level, fluid density, electric power, etc.
Range of main parameters	Core power (max. 8.6 MW), primary pressure (max. about 13.5 MPa), SG secondary-side pressure (max. about 7.3 MPa), primary loop mass flow rate (max. about 15 kg/s), cladding surface temperature (max. about 815 K), etc.
Validation of complete system	1) Experimental data are manually qualified through comparison of published ranges and uncertainty values. 2) Available experimental data are finally obtained by excluding bad trend data among all test data.
Covered phenomena	Single-phase NC, two-phase NC, reflux condensation, liquid level oscillation in SG U-tube due to CCFL, nonuniform flow among SG U-tubes, core two-phase mixture level, core heat transfer, etc.
Covered models	CCFL model, gas-liquid inter-phase drag model, film boiling and steam convective heat transfer model, etc.

Concerning the complete system validation, the experimental data are compared with the published ranges and uncertainty values [5] to manually check the data qualification. Furthermore, bad trend data are excluded from all the experimental data to acquire the available test data.

Several of the covered phenomena and models as well as some of the main parameters over a wide range in the ST-NC-27 test will be explained in Section III *B* and *C*. The ST-NC-27 test satisfied the requirements for the proper SET through the description of the experiment against the foremost criteria as above mentioned. Database obtained from the ST-NC-27 test will be useful for considering safety issues relevant to the CCFL in the PWR.

TABLE III
UNCERTAINTY OF LSTF TEST RESULT FOR EACH OF MAJOR PARAMETERS

Parameter	Uncertainty
Core power	±0.07 MW
Pressurizer pressure	±0.108 MPa
SG secondary-side pressure	±0.054 MPa
Primary loop mass flow rate	±1.25 kg/s
SG inlet plenum collapsed liquid level	±0.185 m
SG U-tube collapsed liquid level	±0.41–44 m
Differential pressure between SG U-tube inlet and outlet	±0.29 kPa
SG U-tube fluid temperature	±2.75 K
Upper plenum collapsed liquid level	±0.197 m
Core collapsed liquid level	±0.216 m
Cladding surface temperature	±5.31 K

III. EXPERIMENTAL CONDITIONS AND RESULTS

A. LSTF Test Conditions

The core power was at a constant value corresponding to 8% of the volumetric-scaled PWR nominal power in which the radial power profile was supposed to be flat. The SG secondary-side collapsed liquid level was maintained at a certain liquid level above the SG U-tube height. The primary and SG secondary-side pressures were represented by the pressures at the vessel upper plenum and at the SG steam dome, respectively. The primary loop mass flow rate is measured by utilizing a venturi flow meter at each primary coolant pump suction leg. Steady-state conditions of the primary and SG secondary-side pressures were about 13.5 MPa and about 7.3 MPa respectively, under forced circulation condition of employing the primary coolant pumps. The NC was established in both primary loops after stopping the primary coolant pumps. Under the NC condition, the primary coolant was drained stepwise at a precise flow rate by opening a valve placed in the auto-bleed line that is connected to the pressure vessel bottom.

Table IV shows the primary loop mass inventory versus estimated time chosen from over a period of time to achieve the steady-state of the system in the NC mode at a constant core power of 8%. The estimated time was 3,000–4,500 s, 5,220–6,040 s, 6,220–6,740 s, 6,980–7,520 s, 8,340–9,400 s, 9,960–11,260 s, 11,820–13,420 s, 13,980–15,060 s, 15,620–16,700 s, 20,780–21,080 s, and 22,220–22,320 s, respectively, for the primary loop mass inventories of 100%, 90%, 88%, 86%, 77%, 72%, 66%, 60%, 55%, 49%, and 39%.

At 55% mass inventory during two-phase NC, the core power was increased at 1% intervals from 8% to 12%, and then was returned to 8%. The core power levels of 8% and 12% are equivalent to 5.7 MW and 8.6 MW, respectively. At 8% core power during reflux condensation, the primary loop mass inventory was reduced to 49% and then to 39%. At 39% mass inventory during reflux condensation, subsequently, the core power was raised at 1% intervals from 8% until the core was uncovered (to be mentioned in Section III *C*). When the core power was turned off following the core uncovery in reflux

condensation mode, the experiment was terminated.

TABLE IV
PRIMARY LOOP MASS INVENTORY VERSUS ESTIMATED TIME IN NC MODE AT 8% CORE POWER

Primary Loop Mass Inventory	Estimated Time	NC Mode
100%	3,000–4,500 s	Single-phase NC
90%	5,220–6,040 s	Two-phase NC
88%	6,220–6,740 s	Two-phase NC
86%	6,980–7,520 s	Two-phase NC
77%	8,340–9,400 s	Two-phase NC
72%	9,960–11,260 s	Two-phase NC
66%	11,820–13,420 s	Two-phase NC
60%	13,980–15,060 s	Two-phase NC
55%	15,620–16,700 s	Two-phase NC
49%	20,780–21,080 s	Reflux condensation
39%	22,220–22,320 s	Reflux condensation

B. NC Flow Behavior at Decreased Primary Loop Mass Inventories under High Core Power Condition

Fig. 3 compares the primary and SG secondary-side pressures in the NC mode. The SG secondary-side pressure was the same between loop-A and loop-B. The SG secondary-side pressure was kept almost at 7.3 MPa through the experiment. A gradual decrease continued in the primary pressure until the primary loop mass inventory was lowered to 77% from the 100% initial value. The primary pressure was maintained at around 8 MPa at a fixed core power of 8% thereafter. The primary pressure increased a little with the stepwise rise of the core power from 8%.

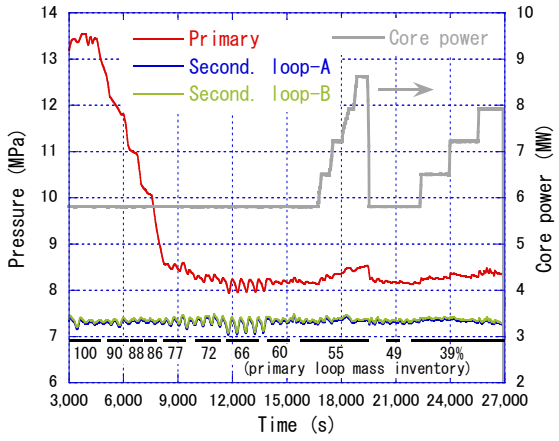

Fig. 3 Measured primary and SG secondary-side pressures and core power in NC mode

Fig. 4 compares the primary loop mass flow rates in the two loops in the NC mode. The primary mass flow rate in loop-A was somewhat different from that in loop-B. Results of the SG U-tube and secondary-side fluid temperatures indicated that the flow in the longer tube was stagnant or reversed (from the SG outlet plenum to the inlet plenum) during single-phase NC, similar to the ST-NC-02 and ST-NC-01 tests [18], [19]. The primary loop mass flow rate was about 11 kg/s at 100% mass inventory of single-phase NC. The normal flow U-tubes made the sufficient primary-to-secondary heat transfer with the well-cooled core. When the primary loop mass inventory was decreased to 90%, the transition occurred from single-phase NC to two-phase NC because the liquid level formed at the hot leg. The primary loop mass flow rate increased with decreasing the primary loop mass inventory because of the larger difference in fluid densities between the upflow and downflow sides of the SG U-tubes due to more steam bubbles. At 72% or 77% mass inventory, the primary loop mass flow rate reached the peak value of about 15 kg/s. Further reduction of the primary loop mass inventory led to a steep decrease of the primary loop mass flow rate with large fluctuation because the steam bubbles formed at the top of the SG U-tubes. At 49% mass inventory, the NC mode changed to reflux condensation mode because a significant level drop started in the SG inlet plenum (to be presented in Figs. 6 and 9) and the primary loop mass flow rate became almost zero. As the core power rose from 8% to 12% at 55% mass inventory during two-phase NC, the primary loop mass flow rate gained with considerable variation because the void fraction increased in the core. As the core power rose from 8% to 11% at 39% mass inventory during reflux condensation, the magnitude of the primary loop mass flow rate oscillation gained.

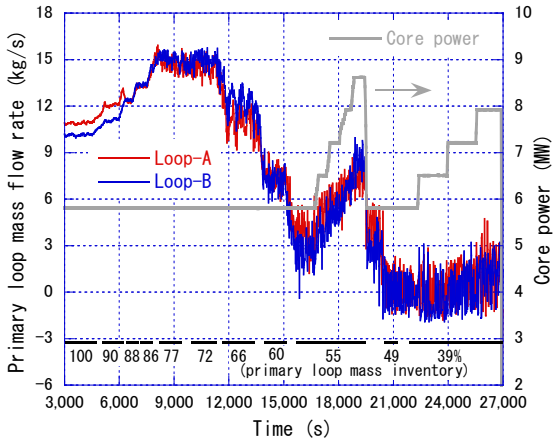

Fig. 4 Measured primary loop mass flow rate and core power in NC mode

Fig. 5 presents the relationship between the primary loop mass inventory and the primary loop mass flow rate (as the averaged value at the estimated time shown in Table IV) at the different core power levels. There were some differences in the primary loop mass flow rates between the two loops. Tendencies of the primary loop mass flow rate depending on the NC mode were qualitatively similar to those observed in the ST-NC-02 and ST-NC-01 tests [18], [19]. Under the equivalent mass inventory condition, the primary loop mass flow rate was greater with the higher core power because of the larger steam flow rate. When the core power levels were 8%, 5%, and 2% respectively, reflux condensation mode was attained in the primary loop mass inventories of 49%, 55%, and 62%.

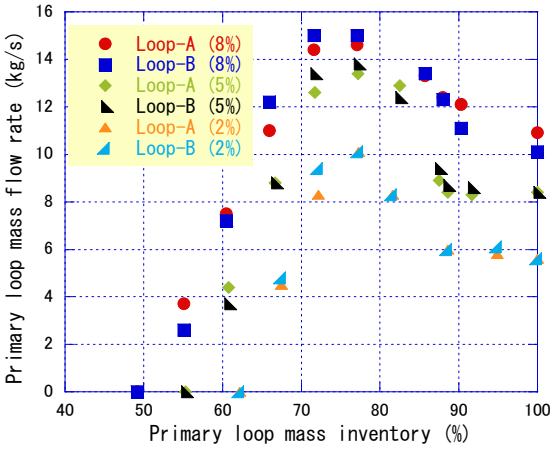

Fig. 5 Measured primary loop mass inventory versus primary loop mass flow rate at different core power levels

C. Influences of Core Power on SG U-Tube Liquid Level Behavior during both Two-Phase NC and Reflux Condensation

The collapsed liquid levels in the SG U-tubes (Tube 1 as the short tube, Tube 2 as the medium tube, and Tube 3 as the long tube mentioned in Table I) respectively are presented in Figs. 6-8 for loop-A, while those are indicated in Figs. 9-11 for loop-B. Figs. 6-11 contain the SG inlet plenum collapsed liquid level and the differential pressure between the SG U-tube inlet and outlet. The collapsed liquid levels in the SG U-tubes and inlet plenum, and the differential pressure between the SG U-tube inlet and outlet were qualitatively the same between loop-A and loop-B. A significant level drop began earlier in the SG short tube than in the SG medium and long tubes. Nonuniform flow distribution was seen among the SG U-tubes. When the core power was increased from 8% at 55% mass inventory during two-phase NC, considerable fluctuation continued in the SG U-tube collapsed liquid levels. When the primary loop mass inventory was 39% at 8% core power during reflux condensation, the SG inlet plenum became empty of liquid (Figs. 6 and 9). Stable liquid holdup took place in the SG U-tube upflow-side owing to the CCFL with high steam velocity and significant condensation of steam at the tube entrance. The SG U-tube downflow-side was not empty of liquid because some steam may flow over the U-tube bend and may condense on the downflow-side. The differential pressure between the SG U-tube inlet and outlet indicated the peak value. When the core power was 9% at 39% mass inventory, the SG inlet plenum collapsed liquid level as well as the differential pressure between the SG U-tube inlet and outlet stayed almost at a certain value (Figs. 6 and 9).

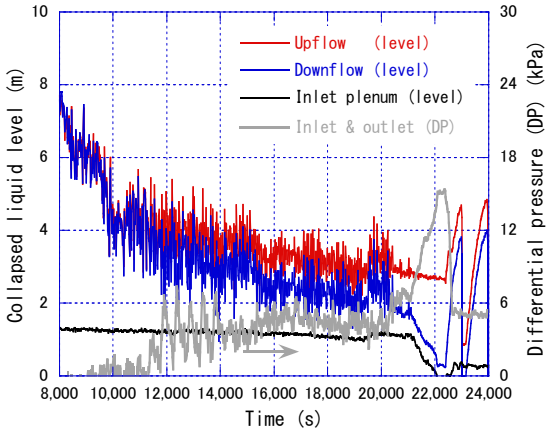

Fig. 6 Measured collapsed liquid levels in SG short tube (Tube 1) in loop-A

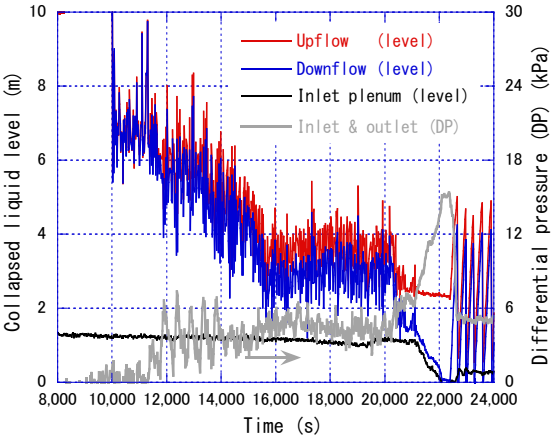

Fig. 7 Measured collapsed liquid levels in SG medium tube (Tube 2) in loop-A

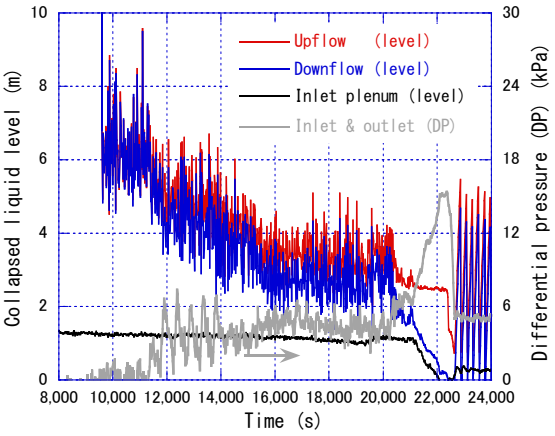

Fig. 8 Measured collapsed liquid levels in SG long tube (Tube 3) in loop-A

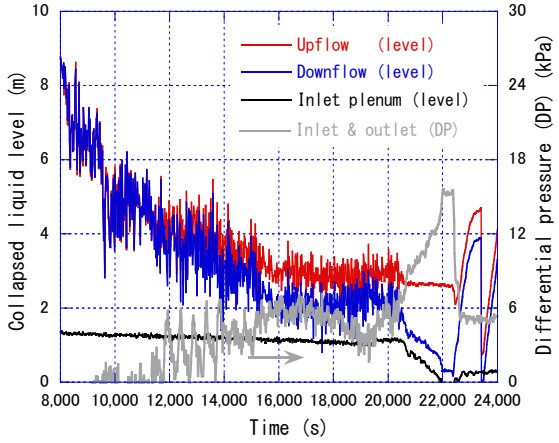

Fig. 9 Measured collapsed liquid levels in SG short tube (Tube 1) in loop-B

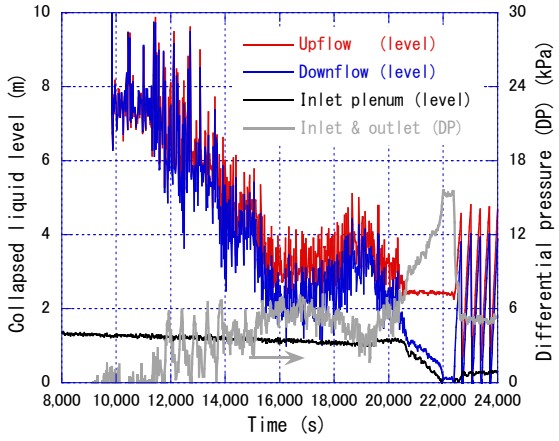

Fig. 10 Measured collapsed liquid levels in SG medium tube (Tube 2) in loop-B

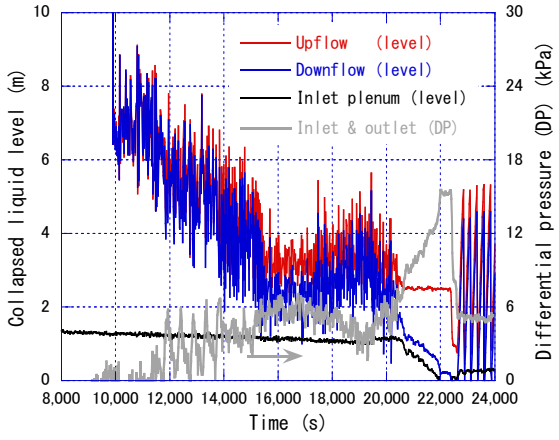

Fig. 11 Measured collapsed liquid levels in SG long tube (Tube 3) in loop-B

Figs. 12-17 respectively present the collapsed liquid levels and fluid temperatures in the SG short, medium, and long tubes at 9-11% core power and 39% mass inventory during reflux condensation typically in loop-A. When the core power was increased from 8% to 9% at 39% mass inventory, the flow distribution in the SG U-tubes became nonuniform. Some differences appeared in the frequency and magnitude of the level oscillation between the two short tubes on account of the effect of different locations (Figs. 12 and 13). For each of the SG medium and long tubes, by contrast, the collapsed liquid levels were similar for the two instrumented tubes (Figs. 14-17). At 9% or more core power and 39% mass inventory, the collapsed liquid levels at the upflow and downflow sides of the SG U-tube slowly increased and dropped in a similar manner owing to the counter balance of water head. Large-amplitude oscillation developed in the void fraction of each SG U-tube rather randomly. The level oscillation timings in a form of slow fill and dump differed for the individual SG U-tubes. The slow fill and dump phenomenon during reflux condensation was comparable to that observed in the LSTF IET [8] concerning the loss-of-feedwater transient without scram with the auxiliary feedwater. In the LSTF IET, the core power and the SG secondary-side collapsed liquid level respectively were fixed to about 7.4% and to about 0.5 m above the SG U-tube bottom for a long time. The cycle of the slow fill and dump in the SG long tube was shorter than that in the SG short tube because of the larger condensate heat transfer area. The cycle of the slow fill and dump at 11% core power was shorter than that at 9% core power because of the larger steam flow rate. The fluid temperatures at the inlet were a little higher than those at the outlet for Tubes 1 and 4 (Figs. 12 and 17), while the fluid temperatures at the inlet were equal to those at the outlet for other instrumented tubes. Therefore, the measured fluid temperatures did not clearly identify the direction of flow in the SG U-tubes during the liquid level oscillation period.

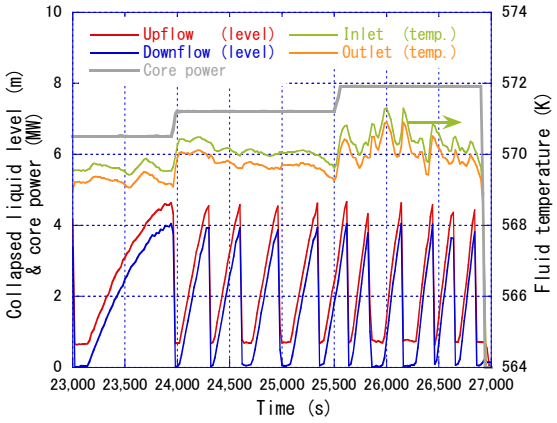

Fig. 12 Measured collapsed liquid levels and fluid temperatures in SG short tube (Tube 1) in loop-A

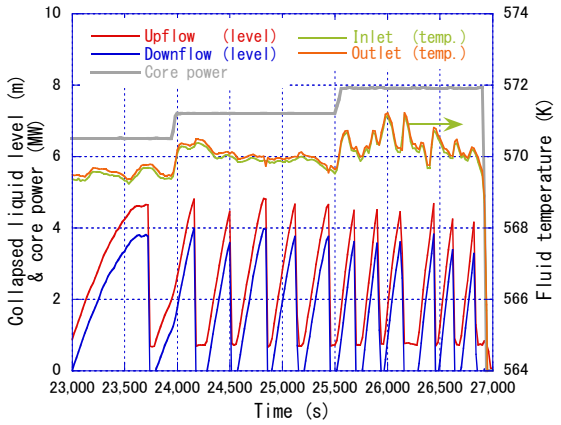

Fig. 13 Measured collapsed liquid levels and fluid temperatures in SG short tube (Tube 6) in loop-A

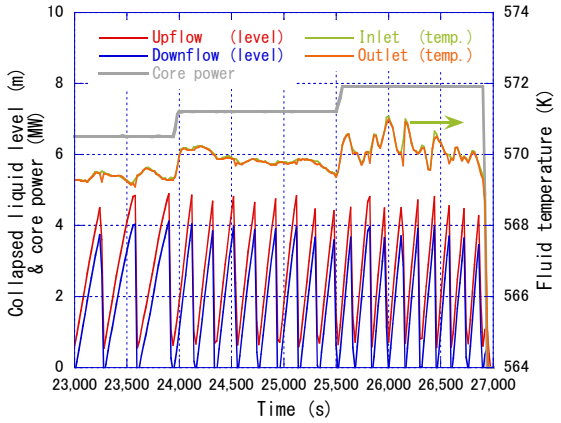

Fig. 14 Measured collapsed liquid levels and fluid temperatures in SG medium tube (Tube 2) in loop-A

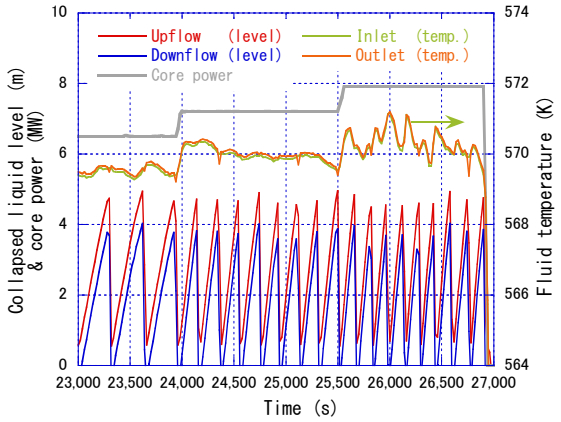

Fig. 15 Measured collapsed liquid levels and fluid temperatures in SG medium tube (Tube 5) in loop-A

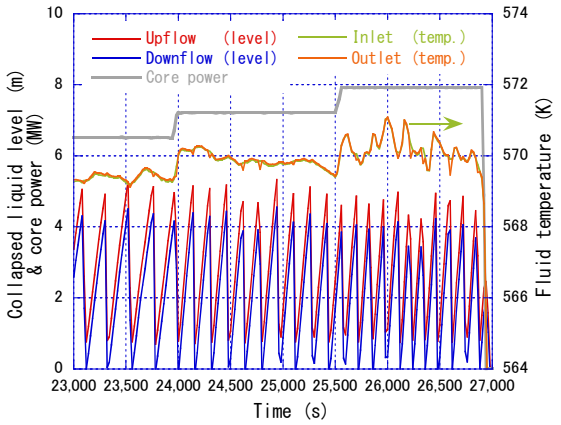

Fig. 16 Measured collapsed liquid levels and fluid temperatures in SG long tube (Tube 3) in loop-A

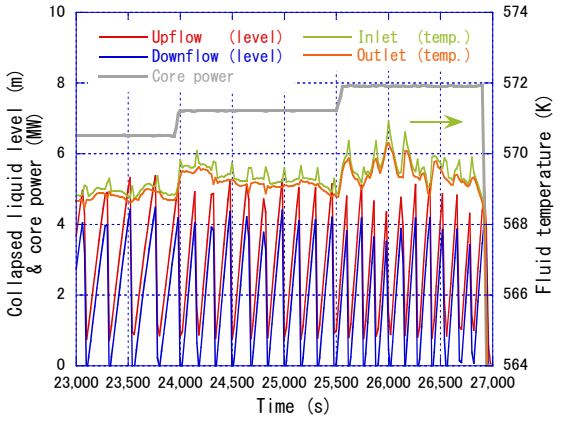

Fig. 17 Measured collapsed liquid levels and fluid temperatures in SG long tube (Tube 4) in loop-A

Fig. 18 shows the collapsed liquid levels in the upper plenum and the core, and the cladding surface temperatures of simulated fuel rods at the different vertical positions, at 39% mass inventory during reflux condensation. The temperature measuring points of Positions 7, 8, and 9 respectively, are located at 2.6 m, 3.0 m, and 3.6 m above the core bottom. The axial distribution of the cladding surface temperature depends on the core collapsed liquid level and the axial power profile. At 8-10% core power and 39% mass inventory, the entire core was covered by two-phase mixture, which resulted in no increase of the cladding surface temperature. At 11% core power and 39% mass inventory, significant drop intermittently occurred in the core collapsed liquid level following the emptying of the upper plenum because the water column developed in the SG U-tubes, which caused intermittent increase of the cladding surface temperature. These suggested that reflux coolant from the SGs should be effective in the core cooling until the core uncovery happened. The peak cladding temperature was about 815 K at Position 8. The core power-off was followed by the whole core quench.

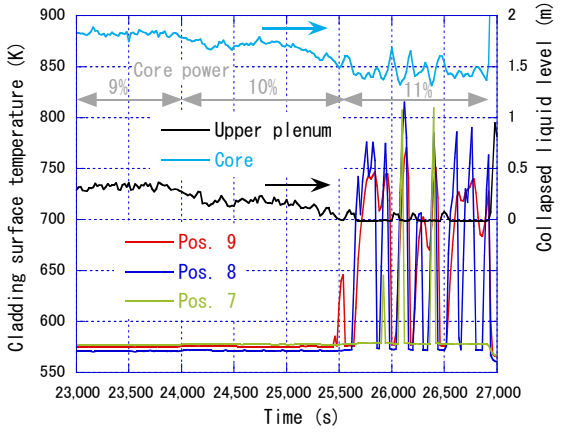

Fig. 18 Measured collapsed liquid levels in upper plenum and core, and cladding surface temperatures

IV. Posttest Analysis by RELAP5 Code

Fig. 19 shows a noding schematic of LSTF system for the posttest analysis with the RELAP5 code. Nine parallel flow channels were applied to the SG U-tubes with nine different lengths to better predict the flow behavior in the SG U-tubes in a nonuniform manner. Specifically, each of four short-to-medium tubes with straight lengths of 9.44–9.89 m (Table I) was divided into 24 nodes, and each of five medium-to-long tubes with straight lengths of 10.04–10.64 m (Table I) was split into 26 nodes.

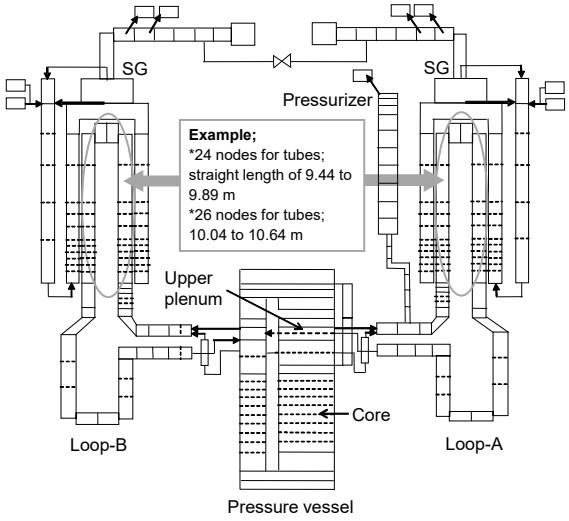

Fig. 19 Noding schematic of LSTF system for RELAP5 code posttest analysis

The following correlation of Wallis was employed to simulate the CCFL at the SG U-tube inlet [26]:

$$j_G^{*1/2} + m j_L^{*1/2} = C, \quad (1)$$

where j^* is the dimensionless volumetric flux. Subscripts G and L express gas and liquid phases, respectively. Slope m and intercept C of the Wallis CCFL correlation at the SG U-tube inlet were set to 1 and 0.75 respectively, by reference to the author's previous work [6]-[8] related to the high-power NC. The SG U-tube inlet was modeled by the junction connecting component for the SG U-tube to that for the SG inlet plenum. The SG secondary-side collapsed liquid level was assumed to be kept at a certain liquid level above the SG U-tube height. The core power and the primary loop mass flow rate assumed were 11% and zero, respectively.

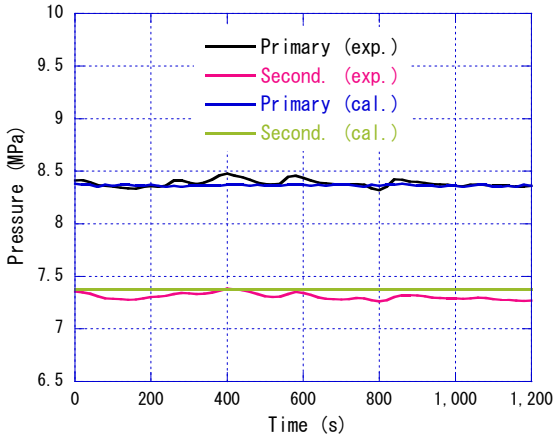

Fig. 20 Test and calculated results for primary and SG secondary-side pressures

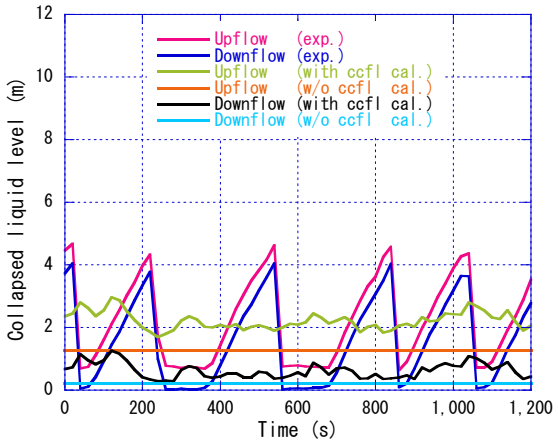

Fig. 21 Test and calculated results for collapsed liquid levels in SG short tube in loop-A

As mentioned in Fig. 20, the calculated primary and SG secondary-side pressures agreed reasonably well with the LSTF test results. Figs. 21-23 respectively present the test and calculated results for the collapsed liquid levels in the SG short, medium, and long tubes typically in loop-A. The test data of the SG short, medium, and long tubes were represented by those of Tubes 1, 2, and 3, respectively. In the calculation, the typical SG short, medium, and long tubes were chosen from the nine parallel flow channels. The calculated values were plotted for

1,200 s after achieving the steady-state of the system, being compared with the test data during the time period of 25,600–26,800 s at 11% core power (as shown in Figs. 12, 14, and 16). In the calculation without using the Wallis CCFL correlation, the collapsed liquid levels at the upflow and downflow sides of the SG U-tubes remained unchanged. The calculated liquid levels at the upflow and downflow sides of the SG U-tubes were somewhat higher than the experimental lowest liquid levels. For the SG medium and long tubes, by contrast, trends of the collapsed liquid levels obtained by the calculation employing the Wallis CCFL correlation were similar to those observed in the experiment. Some discrepancies from the measured data, however, appeared in the frequency and magnitude of the SG U-tube level oscillation probably owing to the difference of the CCFL effect. The large-amplitude level oscillation in the SG short tube was not predicted properly. The code calculated no increase of the cladding surface temperature. The posttest analysis results may imply that coefficients of the Wallis CCFL correlation at the SG U-tube inlet and the nodalization for the SG U-tubes should be modified for better prediction of the SG U-tube liquid level behavior.

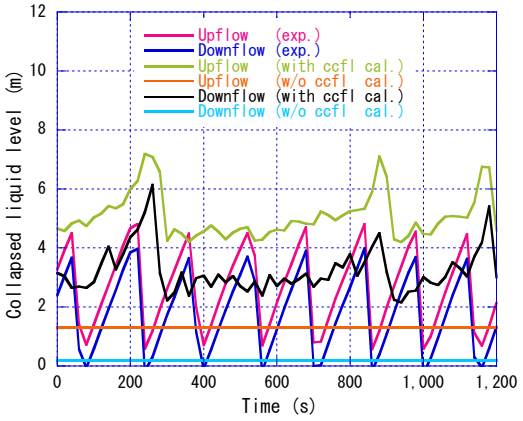

Fig. 22 Test and calculated results for collapsed liquid levels in SG medium tube in loop-A

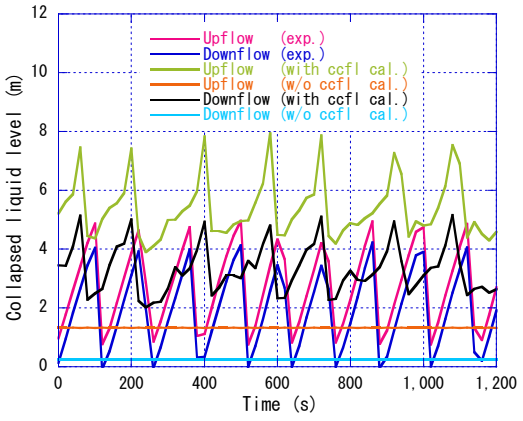

Fig. 23 Test and calculated results for collapsed liquid levels in SG long tube in loop-A

V. Summary

An LSTF SET simulated high-power NC. The SG secondary-side collapsed liquid level was maintained at the certain liquid level above the SG U-tube height. The primary loop mass inventory was decreased stepwise from the 100% initial value at a constant core power of 8% of the volumetric-scaled PWR nominal power. The core power was raised in a stepwise manner from 8% during both two-phase NC and reflux condensation. Moreover, the posttest analysis was conducted with the RELAP5/MOD3.3 code focusing on the SG U-tube liquid level behavior during reflux condensation. The major outcomes are summarized as follows.

When the primary loop mass inventory was reduced to 90% at 8% core power, single-phase NC was replaced by two-phase NC because of liquid level formation at the hot leg. At 72% or 77% mass inventory, the primary loop mass flow rate took the peak. At 49% mass inventory, reflux condensation mode was attained because a significant drop began in the SG inlet plenum collapsed liquid level and the primary loop mass flow rate became almost zero.

When the core power was 8% at 39% mass inventory during reflux condensation, liquid holdup in the SG U-tube upflow-side was stable due to the CCFL and significant condensation of steam at the tube entrance. At 9% or more core power and 39% mass inventory, large-amplitude level oscillation in a form of slow fill and dump took place in the SG U-tubes. At 11% core power and 39% mass inventory, increase intermittently occurred in the cladding surface temperature.

For the SG medium and long tubes other than the SG short tube, the large-amplitude level oscillation with rather randomness was qualitatively reproduced by applying fine-mesh multiple parallel flow channels to the SG U-tubes while employing a Wallis CCFL correlation at the inlet of the U-tubes. However, there were some differences between the test and calculated results for the frequency and magnitude of the level oscillation in the SG U-tubes probably due to the CCFL effect difference.

Acknowledgment

The author would like to thank Messrs. M. Ogawa and A. Ohwada of Japan Atomic Energy Agency for performing the LSTF SET under collaboration with members from Nuclear Engineering Co. as well as Miss K. Toyoda of Research Organization for Information Science and Technology for manipulating the experimental data.

References

[1] H. Shiroyama, “Regulatory failures of nuclear safety in Japan –the case of Fukushima accident,” in: *Proc. of the Earth System Governance Tokyo Conference: Complex Architectures, Multiple Agents, Earth System Governance*, Tokyo, Japan, January 2013.

[2] T. Yonomoto, Y. Anoda, Y. Kukita, and Y. Peng, “CCFL characteristicsof PWR steam generator U-tubes,” in: *Proc. of the ANS International Topical Meeting on Safety of Thermal Reactors*, American Nuclear Society, Portland, Ore, USA, July 1991.

[3] S. Al Issa and R. Macian-Juan, “A review of CCFL phenomenon,” Ann. Nucl. Energy, vol. 38, 2011, pp. 1795–1819.

[4] T. Kusunoki, T. Nozue, K. Hayashi, S. Hosokawa, A. Tomiyama, and M. Murase, “Condensation experiments for counter-current flow limitation

in an inverted U-tube," J. Nucl. Sci. Technol., vol. 53, 2016, pp. 486–495.
[5] The ROSA-V Group, "ROSA-V Large Scale Test Facility (LSTF) System Description for the Third and Fourth Simulated Fuel Assemblies," JAERI-Tech 2003-037, Japan Atomic Energy Research Institute, Ibaraki, Japan, 2003.
[6] T. Takeda, H. Asaka, and H. Nakamura, "Analysis of the OECD/NEA ROSA project experiment simulating a PWR small break LOCA with high-power natural circulation," Ann. Nucl. Energy, vol. 36, 2009, pp. 386–392.
[7] T. Takeda, "Uncertainty analysis of ROSA/LSTF test on pressurized water reactor cold leg small-break loss-of-coolant accident without scram," Int. J. Nucl. Quantum Eng., vol. 13, 2019, pp. 82–90.
[8] T. Takeda, H. Asaka, and H. Nakamura, "RELAP5 analysis of OECD/NEA ROSA project experiment simulating a PWR loss-of-feedwater transient with high-power natural circulation," Sci. Technol. Nucl. Installations, Article ID 957285, vol. 2012, 2012, pp. 1–15.
[9] G.G. Loomis and K. Soda, "Results of the Semiscale Mod-2A natural circulation experiments," USNRC Report NUREG/CR-2335, EGG-2200, Idaho National Engineering Laboratory, 1982.
[10] F. D'Auria and G.M. Galassi, "Characterization of instabilities during two-phase natural circulation in PWR typical conditions," Exper. Therm. Fluid Sci., vol. 3, 1990, pp. 641–650.
[11] P. Basin, R. Deruaz, T. Yonomoto, and Y. Kukita, "BETHSY/LSTF counterpart test on natural circulation in a pressurized water reactor," in: *Proc. of the 1992 National Heat Transfer Conference*, San Diego, CA, USA, August 1992.
[12] Y.M. Ferng and C.H. Lee, "Numerical simulation of natural circulation experiments conducted at the IIST facility," Nucl. Eng. Des., vol. 148, 1994, pp. 119–128.
[13] M. Cherubini, W. Giannotti, D. Araneo, and F. D'Auria, "Use of the natural circulation flow map for natural circulation systems evaluation," Sci. Technol. Nucl. Installations, Article ID 479673, vol. 2008, 2008, pp. 1–7.
[14] A. Del Nevo, F. D'Auria, M. Mazzini, M. Bykov, I.V. Elkin, and A. Suslov, "The design of PSB-VVER experiments relevant to accident management," J. Power Energy Syst., vol. 2, 2008, pp. 371–385.
[15] K. Umminger, L. Dennhardt, S. Schollenberger, and B. Schoen, "Integral Test Facility PKL: Experimental PWR Accident Investigation," Sci. Technol. Nucl. Installations, Article ID 891056, vol. 2012, 2012, pp. 1–16.
[16] V. Kouhia, V. Riikonen, O.P. Kauppinen, et al., "Benchmark exercise on SBLOCA experiment of PWR PACTEL facility," Ann. Nucl. Energy, vol. 59, 2013, pp. 149–156.
[17] J. Kim, K.Y. Choi, K.H. Kang, Y. Park, B.U. Bae, and C.H. Song, "Experimental study for natural circulation flow regime map of ATLAS," *Transaction of the Korean Nuclear Society Spring Meeting*, Jeju, Korea, May 2014.
[18] Y. Kukita, H. Nakamura, K. Tasaka, and C. Chauliac, "Nonuniform steam generator U-tube flow distribution during natural circulation tests in ROSA-IV large scale test facility," Nucl. Sci. Eng., vol. 99, 1988, pp. 289–298.
[19] K. Tasaka, Y. Kukita, Y. Koizumi, M. Osakabe, and H. Nakamura, "The results of 5% small-break LOCA tests and natural circulation tests at the ROSA-IV LSTF," Nucl. Eng. Des., vol. 108, 1988, pp. 37–44.
[20] F. D'Auria and M. Frogheri, "Use of a natural circulation map for assessing PWR performance," Nucl. Eng. Des., vol. 215, 2002, pp. 111–126.
[21] N. Aksan, F. D'Auria, H. Glaeser, R. Pochard, C. Richards, and A. Sjoberg, "Separate Effects Test Matrix for Thermal-Hydraulic Code Validation – Volume I: Phenomena Characterisation and Selection of Facilities and Tests," CSNI report OECD/GD(94)82, 1994.
[22] N. Aksan, F. D'Auria, H. Glaeser, J. Lillington, R. Pochard, and A. Sjoberg, "Evaluation of the CSNI Separate Effects Tests (SET) Validation Matrix," CSNI report OECD/GD(97)9, 1996.
[23] USNRC Nuclear Safety Analysis Division, "RELAP5/MOD3.3 Code Manual," NUREG/CR-5535/Rev 1, Information Systems Laboratories, Inc., 2001.
[24] D. Bestion, F. D'Auria, P. Lien, and H. Nakamura, "A state-of-the-art report on scaling in system thermal-hydraulics applications to nuclear reactor safety," NEA/CSNI/R(2016)14, 2017.
[25] N. Zuber, "Problems in Modeling Small Break LOCA," NUREG-0724, USNRC, Washington, DC, 1980.
[26] G.B. Wallis, "One-Dimensional Two-Phase Flow," McGraw-Hill Book, New York, USA, 1969.

Takeshi Takeda is on loan to Nuclear Regulation Authority from Japan Atomic Energy Agency. His interests include thermal-hydraulic safety during accidents and abnormal transients of light water reactor through experiments using test facilities and by calculations with best-estimate computer code.